A novel BRDF measurement technique with spatial resolution-dependent spectral variance

James R. Shell II, Dr. Carl Salvaggio and Dr. John R. Schott

Digital Imaging and Remote Sensing Laboratory, Center for Imaging Science
Rochester Institute of Technology, 54 Lomb Memorial Drive, Rochester, NY 14623
Email: jrs6394@cis.rit.edu

Abstract— **Overhead spectral imaging has enabled a variety of quantitative remote sensing techniques. However, the derived surface reflectance upon which these techniques rely is generally directional and dependent upon the incident solar and receiving detector angles. The bidirectional reflectance distribution function (BRDF) is becoming increasingly important with the development of non-nadir, multi-angle systems.**

A BRDF measurement approach in the visible to near infrared is described which is suitable for field use. An imaging technique measures BRDF but also enables the generation of the BRDF variability, or the bidirectional reflectance variance function (BRVF). From the measurements, the BRVF and spectral correlation statistics may be produced which are tailored to a sensor's point spread function. Spectral BRDF and BRVF may then be incorporated into spectral algorithms or used for synthetic image generation having accurate spatial and spectral variability, which is of great interest for exercising spectral algorithms.

I. INTRODUCTION

Anisotropic or non-Lambertian reflectance is seldom considered in remote sensing. Incorporating the bidirectional reflectance distribution function (BRDF) improves quantitative results derived from the remote sensing process [1]. Images acquired under varying solar and sensor positions may be normalized by correcting anisotropic reflectance [2]. Better estimates of surface albedo and biophysical properties [3] are made by considering directional reflectance. Improvements to atmospheric correction [4] and spectral classification algorithms [5] are also possible. Remote sensing BRDF models provide the means of estimating the surface leaving radiance for all hemispherical directions and solar zenith positions given a sparse set of observations [3], [6].

Two fundamental approaches to employing BRDF in remote sensing may be made: *i)* deriving the surface BRDF and subsequently surface albedo and biophysical parameters given multi-angle observations [7], [8] or *ii)* using *a priori* BRDF to improve spectral classification and detection algorithms. Use of *a priori* BRDF requires the compilation of BRDF databases for various land cover classes and materials from BRDF field measurements [9]–[11]. However, previously reported measurement techniques do not readily capture the BRDF variability or within-class texture due to the inhomogeneous composition of natural materials. This variability may be quantified by the bidirectional reflectance variance function (BRVF), which is a function of the sensor ground separation distance (GSD). Therefore a BRDF measurement approach is motivated by the need to quantify the BRVF, which is important for higher spatial resolution sensors.

II. BACKGROUND & THEORY

The bidirectional reflectance distribution function (BRDF) quantifies the magnitude and distribution of radiance scattered by a surface and is given by

$$f_r(\theta_i, \phi_i; \theta_r, \phi_r) = \frac{dL_r(\theta_r, \phi_r)}{dE(\theta_i, \phi_i)} \quad (1)$$

where L_r is the surface leaving spectral radiance $\left[\frac{\text{W}}{\text{m}^2 \cdot \text{sr} \cdot \mu\text{m}}\right]$ and E is the incident spectral irradiance $\left[\frac{\text{W}}{\text{m}^2 \cdot \mu\text{m}}\right]$ resulting in BRDF having units of sr^{-1}. The nomenclature is that recommended by Nicodemus [12, Fig. 1], which has been widely adopted where θ_i, ϕ_i are the incident zenith and azimuth angles and θ_r, ϕ_r are the corresponding reflection angles. (Though not always explicitly shown, all radiometric quantities are spectral). Quantifying BRDF is challenging since it is a function of an infinite number of incident and reflection angles, further complicated by a spectral dependence. For practical measurement, the BRDF must be averaged over a finite surface area, A.

The impact of BRDF is understood by considering the radiance sources reaching the sensor. The total radiance in the visible to near infrared (VNIR) (*i.e.* that of solar origin) reaching a sensor may be approximated as the sum of radiance terms having their origin in *i)* direct solar *reflections* (L_r), *ii)* reflected *downwelled* skydome radiance (L_d) and *iii)* *upwelled* radiance from atmospheric scattering along the target-to-sensor path (L_u). The order of the above contributors is typically decreasing in magnitude, though the ground reflectance and atmospheric conditions greatly influence their relative values [13, Fig. 4.12, Tbl. 4.1].

L_r and L_d are given explicitly by[1]

$$L_r = f_r(\theta_i, \theta_r, \phi) E_s(\theta_i') \tau_i(\theta_i') \cos\theta_i' \tau_r(\theta_r', \phi') \quad (2)$$

$$L_d = \iint\limits_{\Omega_i} f_r(\theta_i, \theta_r, \phi) L_d^{\Omega_i'}(\theta_i', \phi_i') \cos\theta_i' \tau_r(\theta_r', \phi') d\Omega_i' \quad (3)$$

---

[1]The most general form of these equations includes polarization, in which case the radiometric flux values are replaced by Stokes vectors, and the scalar BRDF function is replaced by a more general Mueller matrix BRDF representation. This is a topic of current research by the authors.

where the primed coordinate system is the "global" system, or that relative to the normal of the plane of the local earth horizon, and the unprimed coordinates are relative to the individual material surface normals.

The incident exo-atmospheric solar irradiance, E_s, is attenuated by the atmospheric transmittance to the target, τ_i. Similarly, L_d, the reflected downwelled sky radiance is attenuated by τ_r, the transmittance along the target-to-sensor path. The limits of integration encompass the entire hemisphere, or $\Omega_i' = 2\pi \ \text{sr}$ in the earth-based (primed) coordinate system. An explicit function for L_u is not given, as it is not germane to the discussion. Estimates for L_u, $L_d^{\Omega_i'}$, τ_i and τ_s may be obtained through atmospheric propagation codes, such as MODTRAN.

As seen from (2) and (3), BRDF plays a direct role in L_r and L_d; however, the BRDF is usually replaced with a Lambertian approximation such that $f_r \approx \frac{\rho(\lambda)}{\pi}$, where $\rho(\lambda)$ is properly called a reflectance *factor*. (The actual reflectance may only be measured by integrating over the entire hemisphere). Accounting for an anisotropic reflectance factor, or the BRDF, enables the extraction of additional information content.

For homogeneous materials, only a small surface area is required to average out local surface variabilities. However, for heterogeneous surfaces, such as vegetation, a much larger area is required to average out variations. The variability within these material classes is captured by the BRVF [14]. Spatial variance or texture in remote sensing may be quantified in many ways, some of which include frequency domain (Fourier) techniques, autocovariance [15] and "variograms" [16]. Such techniques provide a means of determining the spatial extent over which land cover classes operate.

III. BRDF MEASUREMENT TECHNIQUE

The proposed measurement approach is to use a narrow FOV multispectral imaging system which may be easily repositioned around the scattering hemisphere with a boom or lightweight frame. A focal plane enables BRDF measurement by calculating the average radiance of all pixels, as with a single radiometer, as well as the generation of the BRVF due to the spatial sampling.

Portability for outdoor use and ease of use are key considerations in developing the approach, as are the magnitude of other radiometric uncertainties throughout the remote sensing "imaging chain". One primary uncertainty is the orientation of local surface normals of objects in the scene, an estimate of which is required for applying *a priori* BRDF data to spectral algorithms. The technique sacrifices the angular sampling density of field goniometers, but to the benefit of high portability and the ability to vary the distance (R) to the surface being measured.

The angular resolution of the BRDF measurement, $\Delta\theta_r$ and $\Delta\phi_r$ is limited by and determined from the camera FOV, which becomes an important design criteria. The FOV selection is driven by three interrelated criteria:

1) minimizing the angular averaging, $\Delta\theta_r$ and $\Delta\phi_r$,
2) maximizing the area (A) of the sample measurement and

3) maintaining a reasonable camera to sample distance for ease of repositioning and adjustments.

The importance of criteria 1 is determined by the magnitude of the derivative of the BRDF with respect to θ_r and ϕ_r. Significant changes in the BRDF are characteristic of specular materials near the specular lobe. Fortunately, most natural materials in the VNIR are not appreciably specular. An adequate sample size, A, is determined by the variation or texture scale of that material. The camera to sample distance, R, will mostly drive the ease of repositioning the camera in the hemisphere above the sample. While an increased R may result in decreasing $\Delta\theta_r$ and $\Delta\phi_r$ and/or increases in A, it becomes increasingly difficult to transport, set up and quickly reposition the system. The FOV should also be chosen in conjunction with the uncertainty in θ_i, or the extent of solar zenith movement during a measurement cycle.

A reasonable balance of these requirements is a camera having a $10°$ (full angle) FOV. For nadir viewing ($\theta_r = 0°$) with $R = 6$ ft, this corresponds to a ground area (A) having ≈ 1 ft diameter. This configuration provides an adequate integration area for many materials such as asphalt, grasses and soils, but will be inadequate for shrub and tree canopies. These larger-scale material classes may be measured by increasing the FOV and/or R, or by averaging multiple measurement areas. Criteria for the adequacy of A will be discussed in §IV.

Absolute radiance calibration will be ensured by characterizing the per pixel camera response $g[i,j]$ and imaging a Lambertian calibration surface (image **A**). However, measurement of the calibration target will also contain unwanted contributions from L_d. The L_d contribution may be negated by occluding the solar disk and imaging the calibration target in shadow (image **B**). The L_r radiance may then be determined by **A**-**B**.

Analogous to the manner in which the calibration target was imaged, the image acquired for the BRDF measurement should also be made in full sun (image **C**) and while occluding the sun (image **D**). As before, **C**-**D** isolates the radiance scattered by the direct solar irradiance, assuming no changes in the sky-dome radiance distribution between the measurements. Others have noted similar techniques to compensate for the incident diffuse skydome irradiance [10], [17] and other potential error sources [18].

The strategy for hemispherical sampling must consider the total time required to complete all measurements, as the sun has an angular rate of $15°/\text{hr}$. Changes in the incident solar angle should be kept less than or commensurate with the reflection angle resolution (FOV) or $\Delta\theta_r \approx \Delta\phi \approx 10°$. For materials with azimuthal symmetry, only changes in θ_i need be considered, for which the rate of change is a function of the time of day, year and latitude, reaching a minimum rate at "solar noon" or the maximum sun elevation angle. A total acquisition time of $\lesssim 1$ hr is therefore required for mid-latitude sites. The sequence of events for a BRDF measurement using this technique is summarized in Fig. 1. A wide-FOV RGB image of the skydome is recommended to provide a qualitative assessment of sky conditions.
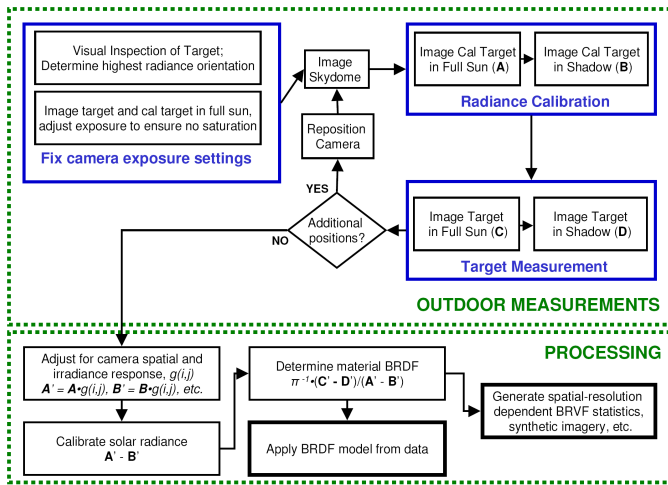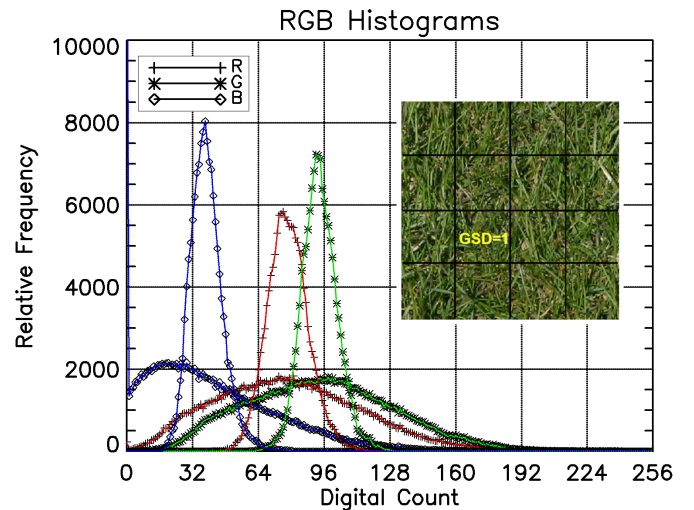
Fig. 1

BRDF MEASUREMENT PROCESS.

Fig. 2

THE RGB COLOR HISTOGRAMS OR BRDF DISTRIBUTIONS FOR A "GRASS" MEASUREMENT USING THE ORIGINAL IMAGE RESOLUTION AND A "GSD = 1" REPRESENTATIVE OF A SPECIFIC SENSOR.

Having acquired data at a single or at most a few θ_i solar positions, with each having a set of sampling locations (~ 20), a means is needed to interpolate to a continuum of θ_i and θ_r, ϕ positions. Empirical interpolation, such as spherical Delaunay triangulation may be used for the specific θ_i under which the measurement was made. However, extrapolation to other θ_i positions warrants the use of an appropriate BRDF model. The data may be used to fit kernel coefficients of land cover BRDF models, such as Roujean's [2], which are then used to estimate the BRDF over the full hemisphere for arbitrary θ_i. Performance comparisons between different models [19], [20] may be used as a basis for specific model selection given the land cover or material attributes.

IV. DETERMINING THE BRVF

The high spatial sampling of the imagery used to determine the BRDF inherently enables extraction of the BRVF. The GSD-dependence of BRVF is illustrated with a hypothetical BRDF measurement of "grass" at a single orientation, shown by the image inset in Fig. 2. This 400×400 pixel image has an average digital count for the 8-bit R, G and B channels of 78.86, 94.40 and 33.31, which is proportional to the BRDF per the process defined by Fig. 1. Examining the histogram of the image reveals the BRVF by showing the BRDF distribution for each spectral band in the 160,000 pixel image. Using this image, the BRVF for a range of GSD values may be computed by convolution of the BRDF image with the sensor point spread function (PSF).

Consider a specific sensor with a normalized GSD unit as shown in Fig. 2. The BRVF may be computed by

$$g[x,y] = \frac{1}{X^2} \sum_{i=0}^{m-1} \sum_{j=0}^{n-1} f[x,y] \, h[x-i, y-j] \quad (4)$$

where $f[x,y]$ is the image and $h[x,y]$ is a convolution kernel.

For this simple example, an ideal low-pass filter kernel of 100×100 pixels is used (GSD = 1 in the Fig. 2). Ideally, $h[x,y]$ is the PSF of the sensor (*e.g.*, an Airy disk pattern) which enables a more accurate BRVF representation.

The histogram resulting from the convolution of the 100×100 kernel in Fig. 2 illustrates the variability reduction for grass imaged at this GSD. The $g[x,y]$ histograms may then be used as the BRVF data. The rate of convergence of the standard deviation of these distributions as a function of GSD may be used as a metric to determine when a sufficient sample size has been imaged to integrate out high frequency inhomogeneities for purposes of the BRDF measurement.

This technique is repeated on each BRDF data set image. Caution is required for BRDF images at high camera zenith angles. The so called "tangent error" effect results in a changing GSD within the FOV of the image. The y-axis or top-to-bottom tangent error effect is given by

$$GSD_y = R \cos \theta_r \left[\tan\left(\theta_r + \frac{FOV}{2}\right) - \tan\left(\theta_r - \frac{FOV}{2}\right) \right] \quad (5)$$

For the proposed system with a FOV = $10°$, the effect at an extreme zenith angle, $\theta_r = 60°$, is considered. At this position, the y-axis resolution relative to that at the center of the image frame is 123% at the top ($\theta_r = 65°$) and 89% at the bottom ($\theta_r = 55°$). The y-axis resolution at the center of the frame is modified by a factor of $\frac{1}{\cos 60°} = 2$ relative to the nadir, $\theta_r = 0°$ view.

Finally, the spatial registration accuracy of the image pairs (**A**,**B**) and (**C**,**D**) used to radiometrically calibrate and correct for the L_d contribution should be considered. BRVF errors may be present from poorly-registered images (*e.g.*, tall grass in wind). Note that these errors are limited to BRVF metrics,

and do not impact the BRDF measurement, as long as a sufficient area is imaged. Mis-registration errors may become appreciable when the sensor GSD is commensurate with the BRDF image GSD.

V. APPLICATION

The BRDF data may be directly used in spectral algorithms given the solar and sensor orientation, as seen from the governing equations for the sensor-reaching radiance (2) & (3). The data may also be used to improve the spatial-dependent, within-class texture variability in synthetic image generation (SIG) programs. SIG programs apply first-principles, physics-based approaches toward generating radiometrically accurate imagery which may be used to exercise spectral algorithms [21]. One of the challenges in SIG is accurate spatial texturing of spectral properties within a material class [22]. Often, rendered materials are too spectrally "pristine", resulting in artificial performance enhancements to spectral algorithms. However, the aforementioned measurement provides the ability to autonomously provide concurrent BRDF and spectrally accurate material variability, all tailored to a sensor-specific PSF.

The band-to-band spectral statistics may be incorporated by principle components (PC) analysis in which spectral data are converted into a space where each band is statistically independent, thus enabling the interdependence to be represented as a 2-D spectral covariance matrix. Spectra may then be statistically generated in this space with the appropriate variance, then back-transformed into the original space to yield the correct spectral statistics [23]. However, this method only accommodates unimodal gaussian distributions. Multimodal distributions may be managed by first applying an unsupervised k-means classification, resulting in spectrally-similar sub-classes [13, §7.2.3] which are typically unimodal. Each of these sub-classes may then be treated by the PC analysis approach.

All these data may be pre-computed prior to the more extensive computation required for rendering a scene in a SIG program. The requisite inputs are the i) processed BRDF image files ($\frac{\mathbf{C}'-\mathbf{D}'}{\mathbf{A}'-\mathbf{B}'}$, cf. Fig. 1), ii) the BRDF model type and coefficients (to inter- or extrapolate to an appropriate θ_i) and iii) the sensor PSF and altitude.

VI. CONCLUSION

A BRDF measurement technique has been proposed which implicitly enables the generation of the BRVF as a function of specific-sensor PSF. The use of such BRDF and BRVF spectral databases provides a means of improving spectral algorithm performance. The generation of synthetic imagery from the data provides an automated means of spatial texture correlation, while retaining the spectral correlation statistics.

DISCLAIMER

The views expressed in this article are those of the authors and do not reflect the official policy or position of the U. S. Air Force, Department of Defense, or the U. S. Government.

REFERENCES

[1] S. Liang, A. H. Strahler, *et al.*, "Multiangle remote sensing: Past, present, future," *Rem. Sens. Rev.*, vol. 18, pp. 83–102, 2000.

[2] J. Roujean, M. Leroy, and P. Deschamps, "A bidirectional reflectance model of the earth's surface for correction of remote sensing data," *J. of Geoph. Res.*, vol. 97, no. D18, pp. 20,455–20,468, December, 20 1992.

[3] N. S. Goel and R. L. Thompson, "A snapshot of canopy reflectance models and a universal model for the radiation regime," *Rem. Sens. Rev.*, vol. 18, pp. 197–226, 2000.

[4] B. Hu, W. Lucht, and A. H. Strahler, "The interrelationship of atmospheric correction of reflectances and surface BRDF retrieval: a sensitivity study," *IEEE Trans. Geosci. Remote Sensing*, vol. 37, no. 2, pp. 724–738, March 1999.

[5] S. Sandmeier and D. W. Deering, "Structure analysis and classification of boreal forests using airborne hyperspectral BRDF data from ASAS," *Rem. Sens. of Env.*, vol. 69, no. 3, pp. 281–295, September 1999.

[6] A. H. Strahler, "Vegetation canopy reflectance modeling–recent developments and remote sensing perspectives," *Rem. Sens. Rev.*, vol. 15, pp. 179–194, 1997.

[7] M. Leroy, J. L. Deuzé, *et al.*, "Retrieval of atmospheric properties and surface bidirectional reflectances over the land from POLDER (processing algorithms)," *J. of Geoph. Res.*, vol. 102, no. D14, pp. 17 023–17 037, July 27 1997.

[8] C. B. Schaaf, F. Gao, *et al.*, "First operational BRDF, albedo nadir reflectance products from MODIS," *Rem. Sens. of Env.*, vol. 83, no. 1–2, pp. 135–148, November 2002.

[9] D. W. Deering and P. Leone, "A sphere-scanning radiometer for rapid directional measurements of sky and ground radiance," *Rem. Sens. of Env.*, vol. 19, no. 1, pp. 1–24, February 1986.

[10] S. R. Sandmeier, "Acquisition of bidirectional reflectance factor data with field goniometers," *Rem. Sens. of Env.*, vol. 73, no. 3, pp. 257–269, September 2000.

[11] P. Nandy, K. Thome, and S. Biggar, "Characterization and field use of a CCD camera system for retrieval of bidirectional reflectance distribution function," *J. of Geoph. Res.*, vol. 106, no. D11, pp. 11 957–11 966, June 16 2001.

[12] F. E. Nicodemus, J. C. Richmond, *et al.*, "Geometrical considerations and nomenclature for reflectance; NBS Monograph 160," Department of Commerce, National Bureau of Standards, Tech. Rep., 1977.

[13] J. R. Schott, *Remote Sensing: The Image Chain Approach*. Oxford University Press, 1997.

[14] W. Ni, C. E. Woodcock, and D. L. B. Jupp, "Variance in bidirectional reflectance over discontinuous plant canopies," *Rem. Sens. of Env.*, vol. 69, no. 1, pp. 1–15, July 1999.

[15] D. L. B. Jupp, A. H. Strahler, and C. E. Woodcock, "Autocorrelation and regularization in digital images. I. Basic theory," *Geoscience and Remote Sensing, IEEE Trans. on*, vol. 26, no. 4, pp. 463–473, July 1988.

[16] C. E. Woodcock, A. H. Strahler, and D. L. B. Jupp, "The use of variograms in remote sensing, I. Scene models and simulated images," *Rem. Sens. of Env.*, vol. 25, pp. 323–348, 1988.

[17] A. I. Lyapustin and J. L. Privette, "A new method of retrieving surface bidirectional reflectance from ground measurements: Atmospheric sensitivity study," *J. of Geoph. Res.*, vol. 104, no. D6, pp. 6257–6268, March 27 1999.

[18] G. F. Epema, "Studies of errors in field measurements of the bidirectional reflectance factor," *Rem. Sens. of Env.*, vol. 35, pp. 37–49, 1991.

[19] Y. Boucher, H. Cosnefroy, *et al.*, "Comparison of measured and modeled BRDF of natural targets," in *Targets and Backgrounds: Characterization and Representation V*, ser. Proc. SPIE, vol. 3699, 1999, pp. 16–26.

[20] O. Hautecoeur and M. Leroy, "Intercomparison of several BRDF models for the compositing of spaceborne POLDER data over land surfaces," in *Intl. Geosc. and Rem. Sens. Symp.*, vol. 1, 1996, pp. 204–208.

[21] J. R. Schott, S. D. Brown, *et al.*, "An advanced synthetic image generation model and its application to multi/hyperspectral algorithm development," *Canadian J. of Rem. Sens.*, vol. 25, no. 2, June 1999.

[22] S. D. Brown and J. R. Schott, "Characterization techniques for incorporating backgrounds into DIRSIG," in *Targets and Backgrounds VI: Characterization, Visualization, and the Detection Process*, ser. Proc. SPIE, vol. 4029, July 2000, pp. 205–216.

[23] J. R. Schott, C. Salvaggio, *et al.*, "Incorporation of texture in multispectral synthetic image generation tools," in *Targets and Backgrounds: Characterization and Representation*, ser. Proc. SPIE, vol. 2469, 1995, pp. 189–196.